Effect of non-phosphorus corrosion inhibitors on biofilm

pore structure and mechanical properties

1

2

3 4 Conghui Huang¹, Peter P. Sun¹, Jungeun Won², Yin Wang³, Stephen A. Boppart^{2,5}, Thanh H. 5 Nguyen*1,4,5 6 7 8 1. Department of Civil and Environmental Engineering, University of Illinois at Urbana-9 Champaign, Urbana, Illinois, 61801, United States 2. Departments of Electrical and Computer Engineering and Bioengineering 10 11 Beckman Institute for Advanced Science and Technology, University of Illinois at 12 Urbana-Champaign, Urbana, Illinois, 61801, United States 13 3. Department of Civil and Environmental Engineering, University of Wisconsin – 14 Milwaukee, Milwaukee, Wisconsin, 53201, United States 15 4. Institute of Genomic Biology, University of Illinois at Urbana-Champaign, Urbana, 16 Illinois, 61801, United States 5. Carle Illinois College of Medicine, University of Illinois at Urbana-Champaign, Urbana, 17 Illinois, 61801, United States 18 19 20 21

Abstract

22

23

24

25

26

27

28

29

30

31

32

33

34

35

36

37

38

39

40

41

Understanding the effects of biofilm structural and mechanical properties, which can influence biofilm cohesiveness and detachment under physical stress, is critical for biofilm and biofilmassociated pathogen control. In this study, we used optical coherence tomography (OCT) and nanoindentation to determine the role of silicate and tin (two experimental non-phosphate corrosion inhibitors) on the porous structure and stiffness of three types of multi-species biofilms. These biofilms were grown from groundwater (a drinking water source), and this groundwater was amended with either tin or silicate corrosion inhibitor (0.5 mg/L as Sn and 20 mg/L as SiO₂). Based on the elastic moduli of these biofilms, tin biofilms and groundwater biofilms were the stiffest, followed by silicate biofilms. The thickness normalized by the growth time for silicate biofilms was highest at $38 \pm 7.1 \,\mu\text{m/month}$, compared to $21 \pm 3.2 \,\mu\text{m/month}$ and 11 ± 2.4 µm/month for tin biofilms and groundwater biofilms, respectively. The silicate biofilms had the greatest overall porosities and thickest among the three biofilms. Based on the pore network modeling (PNM) of OCT images, larger pores and connections were found in the silicate biofilms compared to tin and groundwater biofilms. Our analysis showed that the thicker and more porous biofilms (silicate biofilms) were potentially less resistant to deformation than the thinner and denser biofilms (tin and groundwater biofilms).

Introduction

42

43

44

45

46

47

48

49

50

51

52

53

54

55

56

57

58

59

60

61

62

63

64

Biofilms, a porous matrix developed by microorganisms accumulating on a surface, are ubiquitous in drinking water distribution systems (DWDS).¹⁻⁵ They also play an important role in opportunistic pathogen survival and propagation in both large-scale DWDS and small-scale premise plumbing systems. About 60% of infections by Legionella, an opportunistic pathogen commonly found in premise plumbing, was attributed to the lack of disinfectants, which can be depleted during contact with the biofilm matrix. The presence of biofilms in DWDS can also cause color and taste problems in the drinking water.² Multiple factors in the distribution systems contribute to biofilm growth in drinking water. Hydrodynamic conditions, such as pressure changes induced by the daily water use pattern and stagnation zone at the end of the distribution systems, can play a role in biofilm release and development on the pipe surfaces. Water quality characteristics such as organic matter and disinfectants were used to control biofilms or microorganism regrowth in drinking water.⁸⁻¹⁰ Corrosion inhibitors, which are commonly added into drinking water due to aging DWDS to reduce lead and copper levels in drinking water, are usually phosphate-based and can provide nutrients to microorganisms grown inside the premise plumbing systems. 11 The application of non-phosphate corrosion inhibitors can be a potential alternative to balance the goals between corrosion control and microbial regrowth in DWDS. Non-phosphate corrosion inhibitors such as silicate and tin were reported to reduce the soluble metal (lead, copper, and zinc) leaching from the distribution systems pipes by raising the pH or forming protective layers on the inner pipe surface. 12-15 However, few studies have characterized the biofilm growth under the influence of these corrosion inhibitors.

Knowledge of the pore structure and stiffness of the biofilm matrix is important to understand the effect of the non-phosphate corrosion inhibitors on biofilm growth and release.

Previously, overall biofilm structure (thickness, roughness, porosity, etc.) and development were characterized and monitored by noninvasive imaging techniques such as optical coherence tomography (OCT). 16-20 The pore structure of the biofilms, usually filled with water, can control the transport of nutrients and antimicrobial substances into the biofilm matrix, which is composed of cells and extracellular polymeric substances (EPS).^{21, 22} The spatial distributions of cells and EPS have been characterized by confocal laser scanning microscopy (CLSM) and OCT. ^{20, 23} However, few studies have determined the spatial pore structure. Under shear stress of the water flow, more biofilms and pathogens can be released from biofilms with lower stiffness compared to biofilms with higher stiffness. ²⁴⁻²⁷ However, due to factors such as chemical composition in the feeding water, biofilm age, microbial community structure, and hydrodynamic conditions, a wide range of stiffness (10 - 10⁸ Pa) has been reported.²⁸⁻³¹ This wide range of stiffness implied that biofilms grown under different conditions could demonstrate different resistance when biofilms were exposed to shear stress. Biofilms can also adapt to increasing shear stress by shifting the microbial community structure and EPS composition.³² Although studies showed that the relative porosity could impact the mechanical properties of implants in bone tissue engineering, 33-35 the role of the chemical composition in the feeding water on the biofilm pore structure and stiffness has not been studied. Better control of biomass and pathogens released from biofilms requires an understanding of the biofilm properties developed in drinking water relevant conditions.

65

66

67

68

69

70

71

72

73

74

75

76

77

78

79

80

81

82

83

84

85

86

87

The study objective was to fill the knowledge gap on the effect of non-phosphate corrosion inhibitors on biofilm porous structure and stiffness and the linkage between these biofilm properties. Silicate (sodium metasilicate) and tin (tin sulfate) were chosen to represent a common and experimental non-phosphate corrosion inhibitor, respectively. Groundwater biofilms without

corrosion inhibitors were used as the control. In this study, we 1) characterized the entire structure of bulk biofilms by OCT, a technique that does not require staining; 2) determined biofilm stiffness by nanoindentation; 3) characterized the spatial pore structure of these biofilms by pore network analysis using Avizo (Thermo Fisher Scientific). This is the first study showing that the amendment of non-phosphate corrosion inhibitors led to biofilms with different pore structure and stiffness. Specifically, a more porous biofilm was formed under the influence of silicate corrosion inhibitor compared to that of tin.

Method

1. Biofilm growing conditions

BioSurface Technologies Corporation, Bozeman, MT), a common material in premise plumbing, in three CDC reactors (CBR 90–2, BioSurface Technologies Corporation). These reactors were fed by groundwater, the drinking water source in Urbana-Champaign, IL, after passing through a greensand filter to remove iron and manganese precipitates, similar to filtration at the local drinking water treatment plant. This groundwater was pumped from a well underneath the Newmark Civil Engineering Lab (Urbana, IL) without disinfection treatment. Two non-phosphate corrosion inhibitors: tin (0.5 mg/L as Sn) and silicate (20 mg/L as SiO₂) were chosen to simulate experimental and common alternatives in drinking water, respectively. ^{12, 14} Their concentrations were selected based on those reported in practical applications and lab/pilot-scale investigations. ^{12-14, 36} The groundwater containing silicate was prepared by adding Na₂SiO₃ (Sigma) to 10 L groundwater to reach a final concentration of 20 mg/L as SiO₂. SnSO₄ (Sigma)

was added to 10 L of groundwater to reach a final concentration of 0.5 mg/L as Sn. The groundwater with or without a corrosion inhibitor was prepared freshly every two or three days. The CDC reactors were maintained at 125 rpm (Re = 3510) to simulate the shear stress presented in the DWDS. The feeding groundwater was pumped into the reactors at a flow rate of 1.3 mL/min. The biofilms fed by the groundwater amended with two corrosion inhibitors were grown for six months. The biofilms fed by groundwater were grown for 12 months to allow sufficient biofilm development for nanoindentations. The presence of the bacteria in these biofilms were confirmed by DNA extraction and quantitative polymerase chain reaction (qPCR), as described in Supporting Information (SI).

2. Nanoindentation on biofilms developed with groundwater with or without two corrosion inhibitors

The stiffness of the biofilms fed by groundwater with or without two corrosion inhibitors was determined using a Piuma nanoindenter (Optics11, Amsterdam, the Netherlands). The stiffness was represented by Young's modulus, which represented the deformation of biofilms under physical stress. The greater the Young's modulus, the greater resistance the material had to the deformation under the stress extended by fluid flow. Two to three coupons were taken from each reactor and fixed to the bottom of a 35 mm diameter petri dish by superglue. A pre-calibrated glass probe with a radius of 23.5 or 32.5 μm and a cantilever with stiffness ranging from 0.434 to 0.48 N/m was indented into the biofilms with a maximum limit of cantilever extension of 10 μm. The difference in tip radii was corrected in the calculation of the elastic modulus for the biofilms as shown in **Equation 1**. All indentations were carried out on biofilm-covered coupons submerged in the same groundwater condition that was used to grow these biofilms. The probe was calibrated

in the biofilm feeding water (groundwater and groundwater containing silicate or tin) on a clean bottom of the petri dish before each indentation experiment, following the instrument instructions. The probe was allowed to indent onto the bottom of the petri dish, and the voltage change induced by the bending of the cantilever was monitored and used as a threshold for detection of biofilm surface. If the voltage change was below this threshold, the cantilever was considered to be not bending. This means that if we probe the pores that were filled with water and opened to the surface, the voltage change will be lower than the threshold. The relationship of force and indentation by the probe was measured and recorded by the instrument software, as shown in **Figure S1**. Ten to fifteen locations were randomly chosen on each coupon from each type of biofilm and indented with the probe. A series of approaching velocities of 0.5, 1, 2, or 5 µm/s were used in the indentation profile to access the viscoelasticity of the biofilm stiffness. Indentations were repeated two to three times with the same indentation profile at each location. The contamination of the probe was checked by indenting on a clean petri dish bottom, and the results were compared with the force-distance curves obtained from the calibration of the clean probe. The contaminated probe was washed by isopropanol and water, as instructed by the manufacturer. The distributions of the elastic moduli of these three biofilms were obtained by fitting the force-indentation curves with the Hertz model (Equation 1),³⁷ one of the most common methods to model the nanoindentation experiment with a small range of indentations (less than 10% compared to the sample thickness). 38-40

150
$$F = \frac{4 \times (1 - v)}{3 \times F} \times (R \times d^3)^{1/2}$$
 Equation 1

131

132

133

134

135

136

137

138

139

140

141

142

143

144

145

146

147

148

149

151

152

153

where F is the contact force; R is the tip radius; d is the indentation; v is the Poisson's ratio and assumed to be 0.5 (soft material); E is the elastic modulus. Due to the assumption of shallow indentation (10% of sample thickness) in Hertz's model, the average biofilm thickness should be

greater than 10% of the indentation depth. 41 For this reason, we only subjected biofilms with thickness greater than 90 μ m to nanoindentation. We monitored the thickness of the biofilms over the growing period and found that 12 months were necessary to obtain biofilm thick enough for nanoindentation.

3. OCT imaging and overall biofilm characterization

154

155

156

157

158

159

160

161

162

163

164

165

166

167

168

169

170

171

172

173

174

175

Three coupons were taken out from each reactor for optical coherence tomography (OCT) imaging with a scan dimension of 3.13 mm \times 4.18 mm \times 4 mm. Three randomly chosen locations from each coupon were imaged. For each location, 200 images were taken. Three randomly chosen locations from each coupon were imaged by a custom-built spectral-domain optical coherence tomography (SD-OCT). A superluminescent diode source with a center wavelength and bandwidth of 1310 ± 170 nm (LS2000B, Thorlabs) was used with 1024-pixel InGaAs line-scan camera (SU-LDH2, Goodrich) for detection and a 2D galvanometer scanner (GVS102, Thorlabs) for scanning. The achromatic lens (f = 50 mm, Thorlabs) was used as the objective lens. The system was operated at ~92 kHz line scan rate and had a resolution of ~8 μm and ~20 µm in axial and transverse directions, respectively. More details on OCT schematics can be found from an earlier publication. 42 The cross-sectional biofilm images were pre-processed for orientation corrections using Fiji version 2.00.43 Approximately 100-180 frames in the middle of the stack were selected for overall biofilm structural characterization (Equation 2). In total, over 2000 images were analyzed. The orientation of image stacks was corrected manually by transformation and rotation. The PVC surface in each frame was aligned to the same height along with the scanning direction in the same stack. The coordinates of the PVC surface were determined based on the first frame in each stack. The overall biofilm surface was extracted by

the default auto thresholding using a modified version of the IsoData algorithm by iteratively increasing the threshold to above the composite average of the pixels in the background (at or below threshold) and in the biofilm surface (above threshold). The local biofilm thickness (optical thickness) was determined by subtracting the height of the marked PVC surface from the height of the identified biofilm surface for each cross-sectional image using MATLAB codes, as described previously.^{17, 44} The refractive indices of 1.33 to 1.38 were obtained from three biofilms. The physical biofilm thickness was obtained by dividing the optical thickness by the corresponding refractive index.

$$z(mean) = \frac{1}{n} \times \sum z_i$$
 Equation 2

where z was the local biofilm thickness along the horizontal direction in each OCT frame and n is the number of thickness measurements along the horizontal direction. The normalized thickness of three biofilms were calculated by normalizing the mean biofilm thickness by the growth period of the corresponding biofilms.

4. Biofilm three-dimensional reconstruction and pore structure analysis

We followed the image processing methods used by previous studies, which reconstructed 3D images obtained from porous materials such as rock and soil samples. ^{45, 46} We analyzed five to six locations on each biofilm type. For each imaging location, about 100-180 sequential images in the middle of the stack, which had consistent image quality, were selected for biofilm reconstruction and pore structure analysis. **Figure S2** was representative rendering images obtained from the 3D reconstruction of these OCT image stacks of the tin biofilm. These rendering images were further analyzed to quantify the biofilm porous structure, including the overall porosities, and the pore network model using Avizo. The biofilm matrices containing

both biomass and pore space were created from 5 randomly chosen images among 100-180 images that were obtained along the scanning direction for each OCT stack (one image was selected from every 20-30 images). These biofilm matrices were used to filter out the air-filled space above biofilms. The image analysis included 6 steps, as described in the flow diagram in Figure S3. In step 1, the non-orthogonal angle shift introduced during OCT image collection to reduce water deflection was corrected for the collected images using the Shear module in Avizo. In step 2, the intensity of image slices was adjusted by normalizing the background intensity. In step 3, the images were smoothed and denoised by the Despeckle module. In step 4, the pixel intensity of zero was recognized as the pore space in an image frame using the "Top-hat" function every 280 to 380 µm (15 to 20 frames) apart from the processed stack with 1980 to 3580 µm (100 to 180 frames) depending on the image quality. The results of step 4 could include the pore space outside of the biofilm, and this pore space needed to be removed in steps 5 and 6. In step 5, the biofilm volume was extracted from the whole matrix by automatic thresholding and adjusted by a fill-holes function. Artificial elements created in this step were removed by the 3D erosion module. In step 6, the pores outside the biofilm were removed by subtracting the simulated 3D images created in step 5 from those in step 4. The pores were identified in voxels with an intensity of zero, while the biomass was identified in voxels with non-zero intensity values, as shown in **Figure S2** and **S4**. Over 2000 images were analyzed for these three biofilms. The overall porosity of the biofilms was determined by the ratio between pore and biofilm

198

199

200

201

202

203

204

205

206

207

208

209

210

211

212

213

214

215

216

217

218

219

220

The overall porosity of the biofilms was determined by the ratio between pore and biofilm volume. The pore structure models were constructed based on the connected pores obtained from step 6 using a pore network analysis module in Avizo. The pore volume for each biofilm pore space was characterized by a network generated by a series of theoretically spherical pores connected by cylindrical throats. These pore networks characterized the spatial pore structure

developed under groundwater with or without non-phosphate corrosion inhibitors. The total number of pores and connected throats normalized by the biofilm matrix volume obtained from step 5 and the distributions of pore size and throat length were reported and analyzed. Two pore network analyses were applied to the pore space isolated from each OCT scanned location of two coupons taken from these reactors.

5. Statistical analysis

Statistical comparisons were performed by non-parametric Kolmogorov–Smirnov test and the Wilcoxon rank-sum test using R (version 3.6.2). A bootstrap version of the Kolmogorov–Smirnov test was used when the distributions contained ties.⁴⁷ Percentiles and medians of the dataset were obtained from R. A significant difference was determined by the p-value lower than 0.05.

Results

1. Softest silicate biofilms compared to tin and groundwater biofilms

The effect of time-dependent force on biofilm stiffness was determined by plotting the distributions of elastic moduli over four approaching velocities (**Figure 1**). For all biofilms, the measured stiffness did not significantly change with the approaching velocity (KS test, p > 0.05). The one-year biofilms grown without corrosion inhibitors had a median elastic modulus ranging from 7.5 kPa to 8.9 kPa measured with 0.5 to 2 μ m/s approaching velocities. The 10th and 90th percentile of these groundwater biofilms were 1.4 kPa to 165 kPa, respectively. This range of approaching velocity was chosen because biofilm stiffness obtained from the silicate and tin

biofilms did not significantly change under the approaching velocity ranging from 0.5 to $5 \mu m/s$. Note that the indentation was in the range of 3 to 7 μm deep into the biofilm surface. This thickness is less than 10% of the overall thickness of the biofilm. Therefore, the stiffness measurement was not influenced by the PVC coupons, on which the biofilms were grown. Because the difference in elastic moduli obtained with the approaching velocities in the range of 0.5 to $5 \mu m/s$ was not detected, all three biofilms demonstrated elastic rather than viscoelastic behavior in this range of approaching velocity. In contrast to this observation, single-species biofilms, which were usually cultured within days (instead of over 6 months for tin and silicate biofilms or 12 months for groundwater biofilms) demonstrated more apparent viscous properties than elastic properties at higher frequencies, 48 while elastic properties dominated using indentation at low approaching velocity range. 30

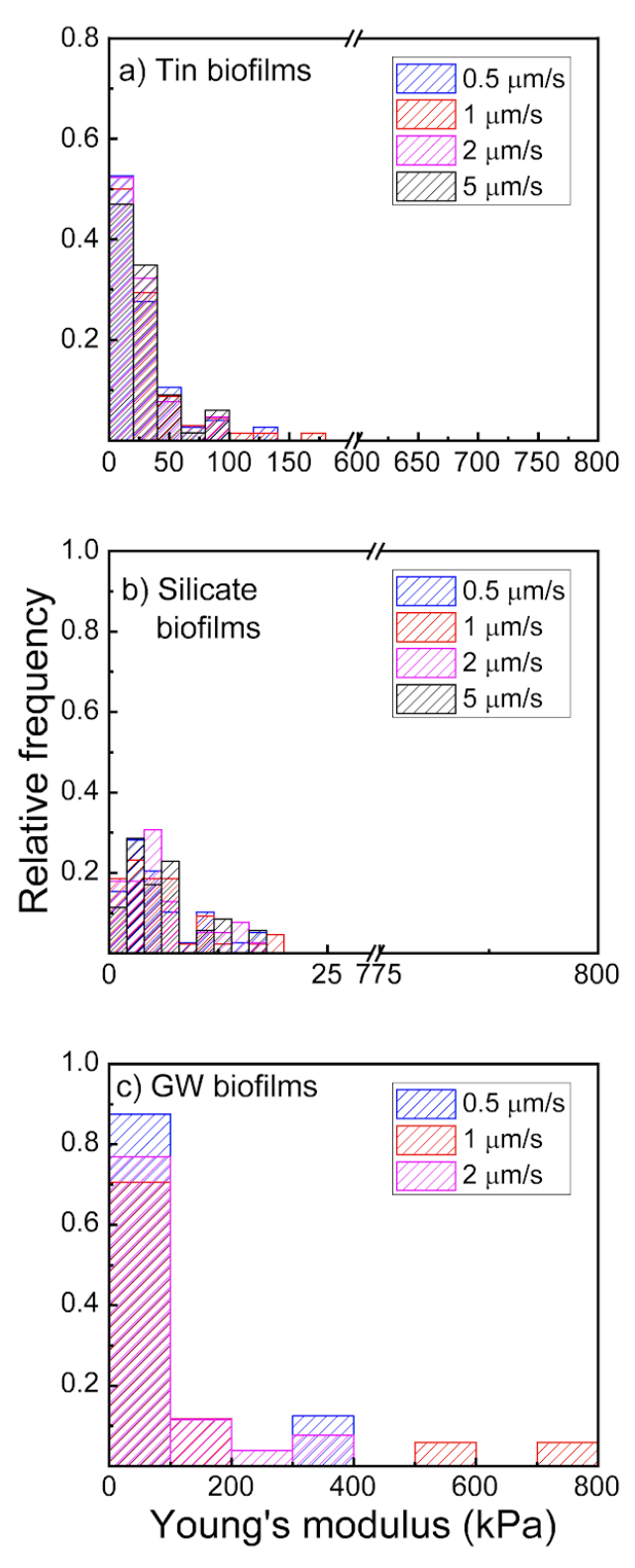


Figure 1. The relative frequency of the measured Young's modulus from **a**) tin biofilms, **b**) silicate biofilms, and **c**) groundwater (GW) biofilms.

We also compared the distribution of elastic moduli obtained from 0.5 to $2~\mu m/s$ for the three types of biofilms as shown in **Figure 2**. The distribution of elastic moduli for these three biofilms was approximated by the log-normal functions. Tin biofilms have significantly greater stiffness than both groundwater and silicate biofilms (KS test, p < 0.05). The median elastic modulus observed from tin biofilms was 19 kPa with 10^{th} and 90^{th} percentiles at 5.9 and 57 kPa, while the median elastic modulus obtained from silicate biofilms was 4.8 kPa with 10^{th} and 90^{th} percentiles at 1.7 and 12 kPa. The median elastic modulus obtained from groundwater biofilms was 7.5 kPa with 10^{th} and 90^{th} percentiles at 1.4 kPa and 165 kPa. Previous studies suggested that stiffer biofilms can be more resistant to biomass release by physical stress. $^{24, 26}$ Among the three studied biofilms, the tin biofilms were the most resistant to deformation and subsequent detachment. Compared with silicate biofilms, groundwater biofilm was likely to resist deformation and detachment.

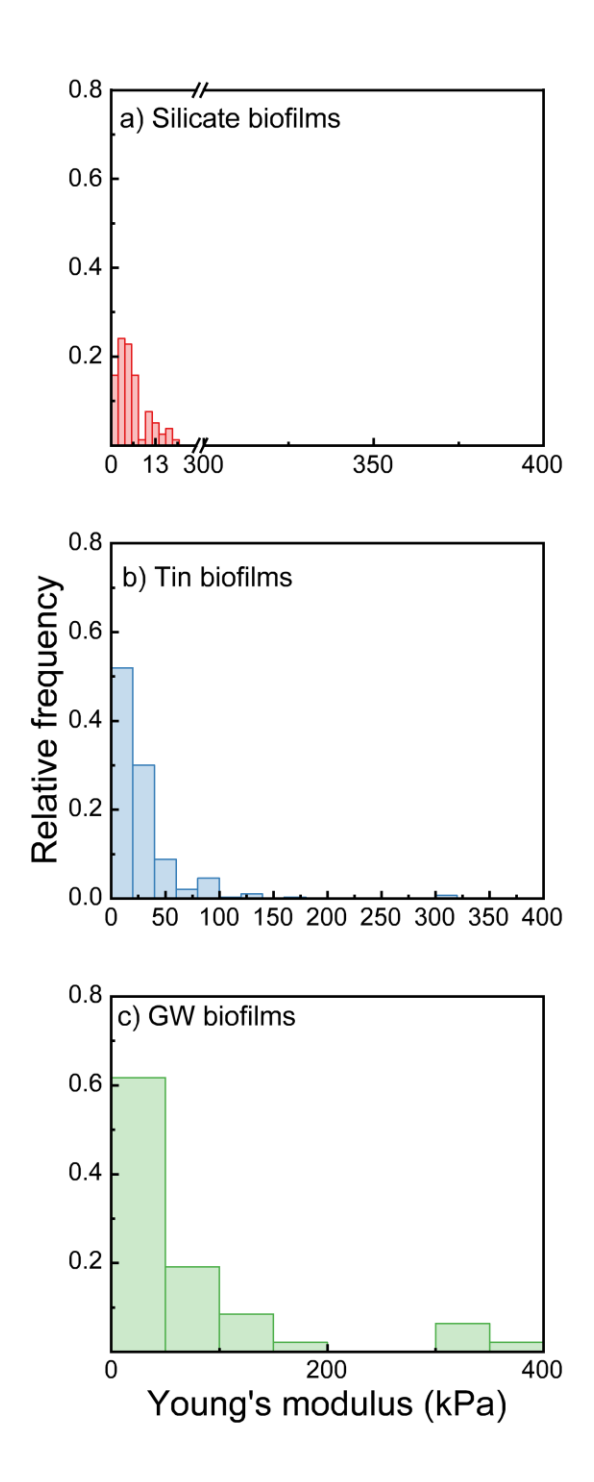


Figure 2. Total relative frequency of the measured Young's modulus from three biofilms: silicate biofilms (**a.** red), tin biofilms (**b.** blue), and groundwater biofilms (**c.** green).

2. Thicker and most porous biofilms developed under groundwater containing silicate corrosion inhibitor

270

271

272

273

274

275

276

277

278

279

280

281

282

283

284

285

286

287

288

289

The average biofilm thicknesses from three biofilms are shown in Figure 3a. The sixmonths silicate biofilms (227 \pm 43 µm) were significantly thicker than the one-year groundwater biofilms (129 \pm 29 μ m), followed by the six-months tin biofilms (126 \pm 19 μ m) based on KS test (p < 0.05). The biofilm thickness normalized by the growth period is shown in Figure 3a. The silicate biofilms developed the most among the three biofilms with a mean normalized thickness of $38 \pm 7.1 \,\mu\text{m/months}$, followed by the tin biofilms with a mean normalized thickness of 21 ± 3.2 um/months. The groundwater biofilms without the corrosion inhibitor additions developed the least with a mean normalized thickness of 11 ± 2.4 μm/months. Previous studies suggested that the silicate-based corrosion inhibitors can prevent the leaching of metal ions into the drinking water by forming a protection layer on the pipe surface. 12, 49, 50 This protective layer formed on the pipe surface can increase surface area and thus can aid in the cell adhesion and biofilm development. 17, 51 Also, silicate biofilms were the most porous with a mean overall porosity of 0.17 ± 0.04 . This porosity is larger than that of the groundwater biofilms without corrosion inhibitor with a mean overall porosity of 0.13 ± 0.05 and tin biofilms with a mean overall porosity of 0.11 ± 0.05 (t-test, p < 0.05) (**Figure 3b**). No significant difference was observed in porosities between the tin and groundwater biofilms (t-test, p > 0.05). In summary, when silicate was used as a corrosion inhibitor, biofilm grown from this amended water was thicker and more porous compared to biofilm grown from groundwater or groundwater containing tin.

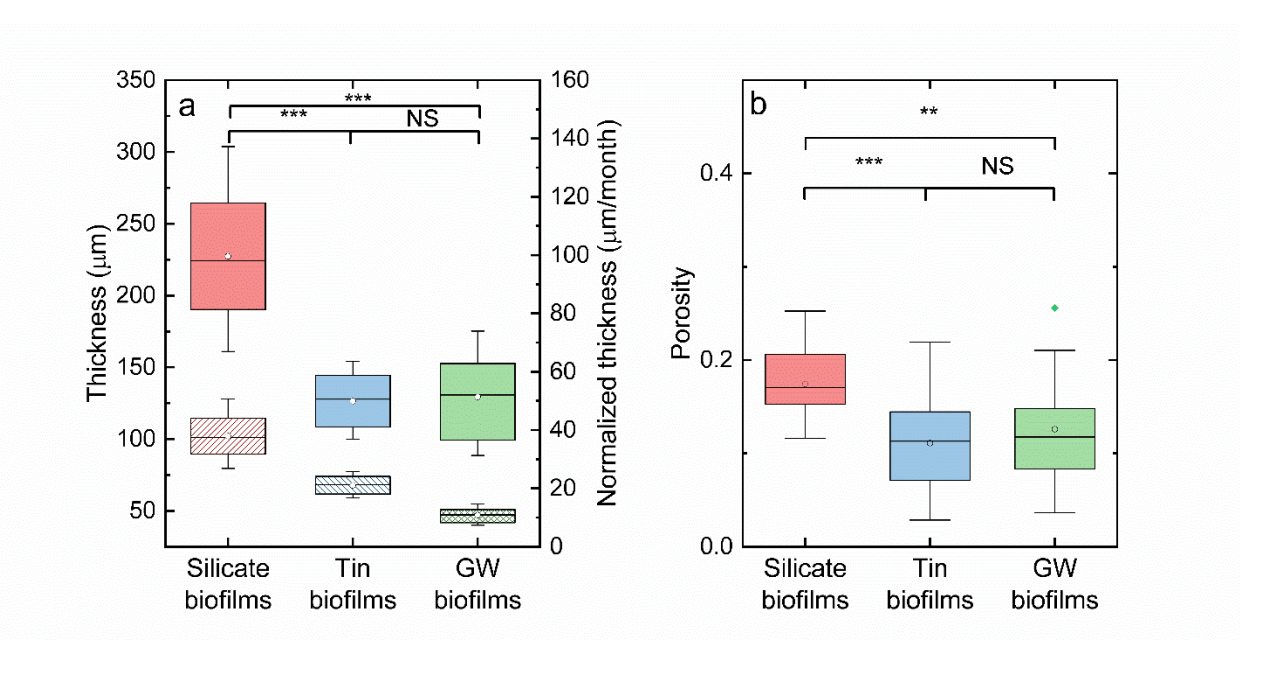


Figure 3. a) Thickness (solid) and normalized thickness (pattern) of silicate, tin, and groundwater biofilms; **b)** Overall porosities of silicate, tin, and groundwater biofilms. Diamond dots indicate the means. The straight lines indicate the median, and the bounds of the colored boxes indicate 25th to 75th percentiles of the distributions. The asterisk indicates that there was a significant difference between two groups of data, as found with a) the Wilcoxon rank-sum test and b) KS hypothesis test. Two asterisks indicated a p-value less than 0.01 while three asterisks indicated a p-value less than 0.001. NS indicated that no significant difference was detected.

3. More large pores and throats were detected for silicate biofilms compared to tin biofilms

The effect of the structure of the pore space in the biofilms, in addition to the overall porosity, was studied by conducting pore network modeling (PNM) based on the OCT images obtained from the three biofilms. In a PNM, the pore space was represented by a series of spherical pores connected by cylindrical throats. Based on the PNM results, we obtained the number of pores and throats and their corresponding size distributions (**Figure 4**). The absolute pore throat number

found in silicate biofilms were the greatest compared to tin and groundwater biofilms. However, silicate biofilms also had the greatest biofilm volume because of the greatest thickness compared to other biofilms. Thus, when we normalized the number of pores and throats of biofilms with the respective biofilm volume, the normalized numbers of pores of these three biofilms were not significantly different (ANOVA, p > 0.05). The numbers of pores per $10^6 \,\mu\text{m}^3$ had a median value of 10 (95% Confidence interval (CI): 5.1-11), 7.2 (95% CI: 3.4-13), and 5.0 (95% CI: 3.5-8.5) for the silicate, tin, and groundwater biofilms, respectively. Despite the similar number of pores detected in three biofilms, the silicate biofilms had significantly more throats than the tin biofilms (KS test, p < 0.05). The numbers of throats per $10^7 \,\mu\text{m}^3$ had a median value of 8.4 (95% CI: 5.4-13), 4.9 (95% CI: 2.2-5.7), and 6.9 (95% CI: 3.5-11) for the silicate, tin, and groundwater biofilms, respectively.

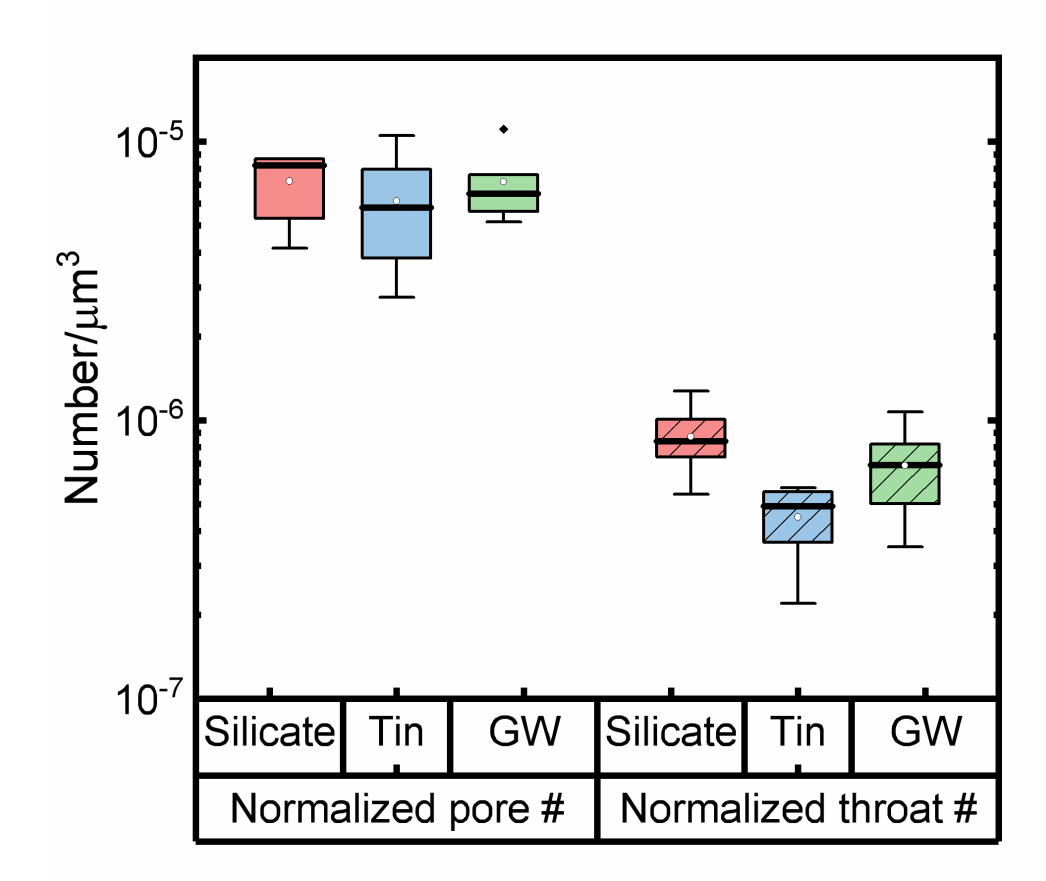


Figure 4. Normalized pore (solid) and throat (dashed) number by biofilms volume of silicate (red), tin (blue), and groundwater (green) biofilms. Points outside of the tail indicate outliers of the data obtained for groundwater (GW) biofilms. This outlier was not observed for other biofilms.

317

318

319

320

321

322

323

324

325

326

327

328

329

330

331

332

333

334

335

336

337

338

339

Because the axial resolution of OCT was around 5-8 µm, we only include the pores and throats with an equivalent radius above 5 µm in our following statistical analysis. The distributions of the pore equivalent radius determined by the PNM for these three biofilms are shown in Figure 5. Among the three studied biofilms, the distribution of the pore equivalent radius was significantly greater in the groundwater biofilms than those in the silicate and tin biofilms (p < 0.05). The median of the pore equivalent radius determined from silicate, tin, and groundwater biofilms is 7.0 $(95\% \text{ CI: } 5.6 - 58 \text{ }\mu\text{m}), 6.9 (95\% \text{ CI: } 5.5 - 55 \text{ }\mu\text{m}), \text{ and } 7.4 (95\% \text{ CI: } 5.1 - 59 \text{ }\mu\text{m}), \text{ respectively.}$ About 2 times more pores with an equivalent radius greater than 100 µm were found in silicate biofilms compared to groundwater biofilms. The median of the pore equivalent radius in groundwater biofilms was greater than that in silicate biofilms. However, more pores were found in silicate biofilms compared to groundwater biofilms in the greater pore equivalent radius range. The distribution of pore equivalent radius found in silicate biofilms was slightly but significantly greater than those in tin biofilms (KS test, p < 0.05). The distribution of the pore equivalent radius in the silicate biofilms showed that about 11 times more pores with a radius greater than 100 µm compared to those in the tin biofilms.

The characteristics of throats connecting the pores are shown in **Figure 6**. The throat equivalent radius was greatest for silicate biofilms with a median of 17 μ m (95% CI: 6.0 – 49 μ m) compared to that in tin biofilms with a median of 15 μ m (95% CI: 6.0 - 40 μ m) and that for groundwater biofilms with a median of 15 μ m (95% CI: 5.9 - 35 μ m) (KS test, p < 0.05). A higher

frequency of throats with larger equivalent radius was detected for silicate biofilms compared to tin and groundwater biofilms. The throat length in silicate biofilms with a median of 193 µm (95%) CI: 78 - 450 µm) was slightly greater compared to those in the tin biofilms with a median of 185 μ m (95% CI: 82 – 416 μ m). The distributions of throat equivalent radius and length showed that more throats in the silicate biofilms had greater and longer connecting throats compared to those found in the other biofilms. About 6 and 24 times more throats with an equivalent radius greater than 65 µm were found in the silicate biofilms than those in the groundwater biofilms and the tin biofilms, respectively. Also, the number of throats in the silicate biofilms with length greater than 700 µm was about 7 times and 5 times more than those in the tin and groundwater biofilms, respectively. More throats connecting the pores instead of isolated pores were also found in the silicate biofilms. Note that silicate biofilms also had a greater overall porosity compared to tin and groundwater biofilms. This greater overall porosity in silicate biofilms can be attributed to the higher detection frequency of larger connections and pores detections. Based on the pore network analysis results of the three biofilms, biofilms developed without corrosion inhibitors had the largest pore but smallest throats among the three biofilms (see Table of Content art).

340

341

342

343

344

345

346

347

348

349

350

351

352

353

354

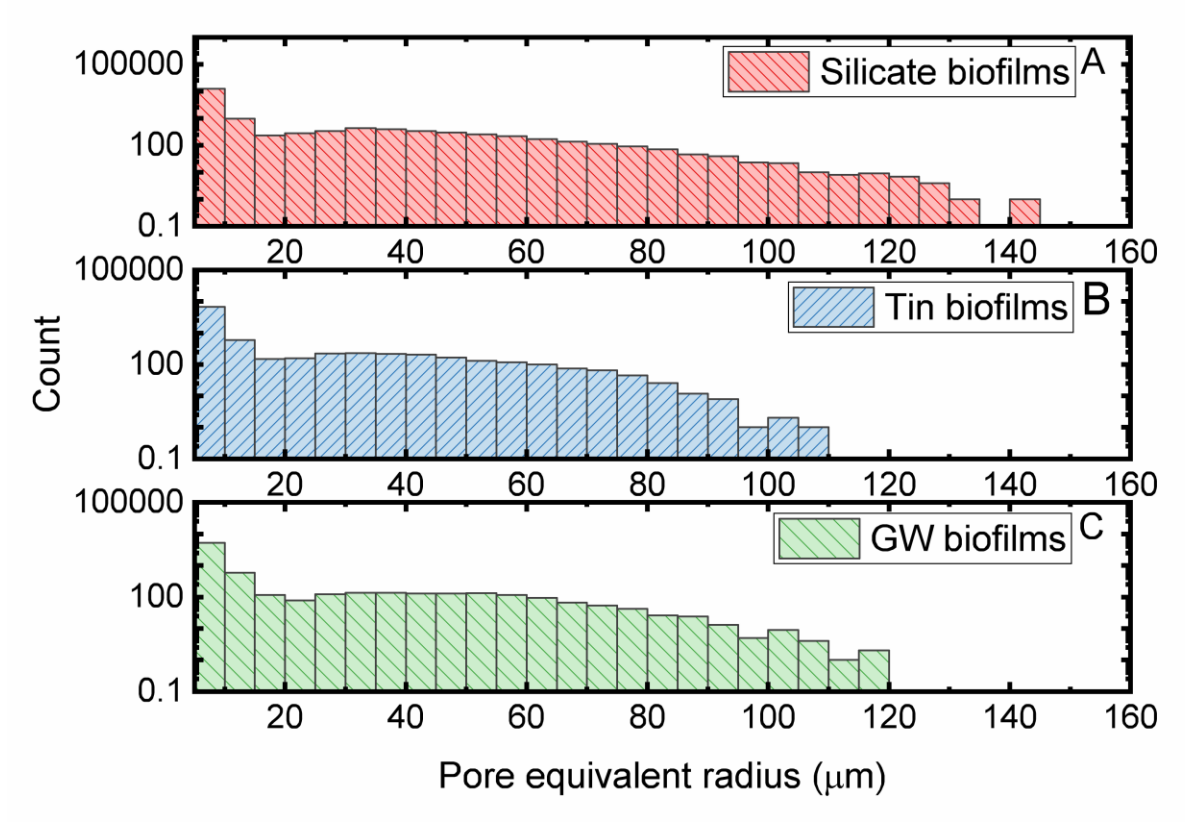


Figure 5. Distributions of pore equivalent radius in silicate (A. red), tin (B. blue), and groundwater (C. green) biofilms.

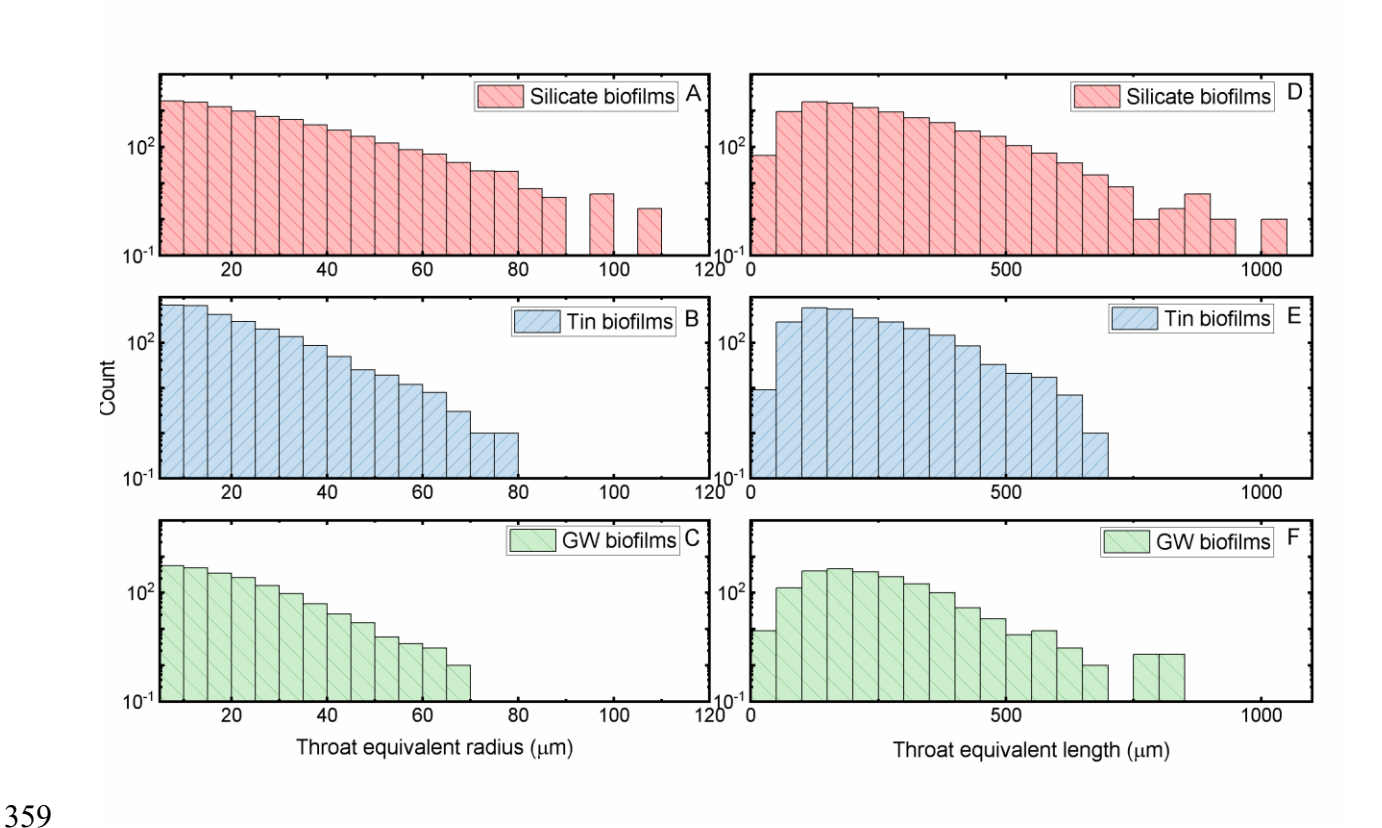


Figure 6. Throat equivalent radius (A, B, and C) and length (D, E, and F) from silicate biofilms (red), tin biofilms (blue), and groundwater biofilms (green).

Discussion

Biofilm detachment has been found to relate to biofilm stiffness.^{24, 26} A wide range of biofilm stiffness (10 - 10⁸ Pa) was reported from single and multi-species biofilms grown on various surfaces.²⁹⁻³¹ It is important to understand how biofilm stiffness can be attributed to the biofilm architecture, chemical composition, and growing conditions. For example, the elastic moduli of two strains of *Pseudomonas aeruginosa* biofilms grown for three days were in the range of 15 to 170 kPa.³⁹ These values were greater than those for silicate and groundwater biofilms but overlapped with tin biofilms. Microcolonies of *P. aeruginosa* developed in three days had the

elastic modulus below 80 Pa.⁵² These stiffness values were much lower than those of the three biofilms in this study, suggesting that young monospecies biofilms of *P. aeruginosa* were less stiff than the mature multi-species biofilms grown from low-nutrient drinking water. Biofilms grown from the same groundwater source in a similar CDC reactor setup had the elastic moduli in the range of 0 to 14 kPa.²⁴ This range overlapped with the elastic moduli of silicate and groundwater biofilms and half of those of tin biofilms. The greater stiffness in tin biofilms showed that using tin corrosion inhibitors can promote a biofilm that have more resistance to physical stress compared to silicate biofilms. The results of this study and our previous study using simulated drinking water suggest that drinking water biofilm stiffness may not be inferred from mono-species biofilms grown over a short time from nutrient-rich conditions.

We showed here that biofilm porous structure and development could adapt to the water chemical composition, which is altered by adding a corrosion inhibitor. We found that the addition of tin or silicate to groundwater led to faster biofilm growth rate on the PVC surface compared to biofilms developed with only groundwater. This faster development of silicate or tin biofilms can be caused by the formation of silicate or tin scales on the PVC surface that increased the surface area for cell adhesion and accumulation. Silicate scale formation on the pipe surface has been reported when silicate was used as a corrosion inhibitor. ^{13, 49, 50} The greater porosity observed with the thicker silicate biofilms can also be explained by the less resistance of nutrients transported through the bulk biofilms. ¹⁸ Significant thicker biofilms with polyphosphate were observed compared to groundwater biofilms, while thin biofilms developed under soft groundwater. ²⁵ Minerals of calcium carbonate, such as calcite and aragonite, in untreated groundwater biofilms, can result in a compact structure and a stiffer matrix compared to polyphosphate and soft groundwater biofilms. ²⁵ The observation of faster biofilm development in the presence of tin or

silicate compared to that fed by only groundwater demonstrated that although two non-phosphate corrosion inhibitors were not considered nutrient for bacteria, their presence can still promote biofilm growth. Pore structure was reported to be correlated with mechanical properties, such as stiffness and compress yield stress, in an engineered porous material.³⁵ The effective Young's modulus reduced with increasing porosity in ceramics.⁵³ However, characterization of both biofilm stiffness and pore structure has not been conducted. Our results revealed that the abundant long or large water-filled connecting throats can contribute to the reduction of force measured during indentation into silicate biofilms under water. The results of this study showed that the presence of silicate and tin as corrosion inhibitors influenced the biofilm structure and stiffness. The biofilms developed under silicate corrosion inhibitor were porous and soft, while those developed under tin corrosion inhibitor were compact and stiff. The stiffer tin biofilms can be more resistant to the shear stress induced by the water flow and less detachment can be expected from tin biofilms compared to softer silicate biofilms.^{25, 26} Also, silicate biofilms can be expected to detach more due to their greatest thickness and fastest development among the three studied biofilms.

Silicate has been commonly used as a corrosion inhibitor in drinking water systems in the U.S. since 1920s.¹³ Silicate may mitigate iron and manganese release through a colloidal dispersion mechanism. The exact mechanism of silicate for lead and copper corrosion control is still uncertain, and previous work suggested that silicate may reduce lead and copper release by raising pH and/or formation of a protective layer on the pipe scales.¹⁴ Tin (Sn)-based corrosion inhibitors are relatively new, and their exact role for corrosion control is still under investigation. Previous research suggested that Sn(II) may be oxidized to Sn(VI), which would mitigate lead release through the formation of low-solubility lead precipitates.³⁶ We also obtained chemical composition of the studied biofilms using Fourier-transform infrared spectroscopy (FTIR) and

Scanning Electron Microscopy (SEM) coupled with Energy Dispersive X-Ray Spectroscopy (EDS). However, we did not get quantitative results that give a clear picture of the chemical composition of the studied biofilms because the signals of other components are so much higher than those from silicate or tin.

Due to the complexity and heterogeneity of the biofilm development on the coupons, we cannot accurately determine the biofilm stiffness in the shear direction in this study. However, the near-surface stiffness measured by the indentations can also demonstrate the resistance to detachment by the shear flow.^{24, 25} The possible biomass detachment by the shear flow for these biofilms and the biofilm microbial composition should be quantified in future studies.

Environmental Relevance

Biofilm development and detachment can cause deterioration of drinking water aesthetics (taste, odor, and discoloration), which was in about 80% of the consumer complaints received by the utilities. 9,54 In addition, consumers can be exposed to opportunistic pathogens in the water when biofilms detach by the water shear stress. About 430 million and 425 million USD of economic costs were estimated for the treatment of infection by the two most common opportunistic pathogens in drinking water, *Legionella* and nontuberculous *Mycobacteria* in the US, respectively. 55 Because these two pathogens have been found in drinking water biofilms, 56-58 knowledge on how to control biofilm detachment could help to improve water quality at the taps. This study is the first to characterize the pore structure and the stiffness of biofilms grown from the groundwater, a source for drinking water, with or without a non-phosphate corrosion inhibitor. Silicate biofilms were thicker with a network of connecting pores, while tin biofilms were thinner with more isolated pores. The water-filled connected pores in silicate biofilms can

438 contribute to the lower stiffness measurements by indentations. Previously, under stress applied 439 by water flow, biofilms with lower stiffness tend to detach more compared to stiffer biofilms.^{24,} 440 ²⁶ The results of this study suggest that using tin instead of silicate as a corrosion inhibitor can 441 potentially reduce biofilm growth and subsequent detachment in the DWDS. 442 Acknowledgments 443 444 We acknowledge partial support from the Zhejiang-Illinois institute and NSF grant 1855609. We 445 thank Dr. Guillermo L. Monroy from University of Illinois at Urbana-Champaign for obtaining 446 the OCT images. We thank the MATLAB code developed in Dr. Nicolas Derlon and Professor 447 Eberhard Morgenroth from the Swiss Federal Institute of Aquatic Science and Technology 448 (Eawag). 449 Supporting information 450 Additional information regarding confirming the presence of bacteria in these biofilms are

- 451
- 452 provided in the supporting information. Figures the representative force-indentation curves, the
- 453 image analysis workflow, and the biofilm 3D reconstruction images are included.

References 455

- 456 Hong, P.-Y.; Hwang, C.; Ling, F.; Andersen, G. L.; LeChevallier, M. W.; Liu, W.-T., 1.
- 457 Pyrosequencing Analysis of Bacterial Biofilm Communities in Water Meters of a Drinking Water
- 458 Distribution System. Applied and Environmental Microbiology 2010, 76 (16), 5631-5635.
- 459 Douterelo, I.; Husband, S.; Loza, V.; Boxall, J., Dynamics of Biofilm Regrowth in
- Drinking Water Distribution Systems. Applied and Environmental Microbiology 2016, 82 (14), 460
- 461 4155-4168.

- Douterelo, I.; Jackson, M.; Solomon, C.; Boxall, J., Microbial analysis of in situ biofilm
- 463 formation in drinking water distribution systems: implications for monitoring and control of
- drinking water quality. *Applied Microbiology and Biotechnology* **2016**, *100* (7), 3301-3311.
- 465 4. Cruz, M. C.; Woo, Y.; Flemming, H.-C.; Wuertz, S., Nitrifying niche differentiation in
- 466 biofilms from full-scale chloraminated drinking water distribution system. Water Research 2020,
- 467 *176*, 115738.
- 468 5. Hallam, N. B.; West, J. R.; Forster, C. F.; Simms, J., The potential for biofilm growth in
- 469 water distribution systems. *Water Research* **2001**, *35* (17), 4063-4071.
- 470 6. Declerck, P., Biofilms: The environmental playground of Legionella pneumophila.
- 471 Environmental Microbiology **2010**, *12* (3), 557-566.
- 472 7. Beer, K. D.; Gargano, J. W.; Roberts, V. A.; Hill, V. R.; Garrison, L. E.; Kutty, P. K.;
- Hilborn, E. D.; Wade, T. J.; Fullerton, K. E.; Yoder, J. S., Surveillance for waterborne disease
- outbreaks associated with drinking water—United States, 2011–2012. MMWR Morb Mortal Wkly
- 475 Rep **2015**, 64 (31), 842-8.
- Wang, H.; Masters, S.; Hong, Y.; Stallings, J.; Falkinham, J. O.; Edwards, M. A.; Pruden,
- 477 A., Effect of Disinfectant, Water Age, and Pipe Material on Occurrence and Persistence of
- 478 Legionella, mycobacteria, Pseudomonas aeruginosa, and Two Amoebas. Environmental Science
- 479 & Technology **2012**, 46 (21), 11566-11574.
- 480 9. Prest, E. I.; Hammes, F.; van Loosdrecht, M. C. M.; Vrouwenvelder, J. S., Biological
- 481 Stability of Drinking Water: Controlling Factors, Methods, and Challenges. Frontiers in
- 482 *Microbiology* **2016,** *7* (45).
- 483 10. LeChevallier, M. W.; Schulz, W.; Lee, R. G., Bacterial nutrients in drinking water. Applied
- 484 and Environmental Microbiology **1991**, *57* (3), 857-862.
- 485 11. Liu, S.; Gunawan, C.; Barraud, N.; Rice, S. A.; Harry, E. J.; Amal, R., Understanding,
- 486 Monitoring, and Controlling Biofilm Growth in Drinking Water Distribution Systems. *Environ Sci*
- 487 *Technol* **2016,** *50* (17), 8954-76.
- 488 12. Hosseinibalajadeh, S. Lead Corrosion Inhibitors in Drinking Water. The University of
- Wisconsin-Milwaukee, 2018.
- 490 13. Thompson, J. L. S., Barry E.; Schock, Michael R.; Lytle, Darren A.; Delaney, Patrick J.
- 491 Sodium Silicate Corrosion Inhibitors: Issues of Effectiveness and Mechanism; American Water
- Works Association: Water Quality Technology Conference, 1997.
- 493 14. Schock, M. R.; Lytle, D. A.; Sandvig, A. M.; Clement, J.; Harmon, S. M., Replacing
- 494 polyphosphate with silicate to solve lead, copper, and source water iron problems. *Journal AWWA*
- 495 **2005,** *97* (11), 84-93.
- 496 15. Hozalski, R. M. T., Ying; Dai, Xiaojun Investigation of stannous chloride as an inhibitor
- 497 of lead corrosion. Water Research Foundation; Water Research Foundation: 2010.
- 498 16. Neu, L.; Proctor, C. R.; Walser, J.-C.; Hammes, F., Small-Scale Heterogeneity in Drinking
- Water Biofilms. Frontiers in microbiology 2019, 10, 2446-2446.
- 500 17. Shen, Y.; Monroy, G. L.; Derlon, N.; Janjaroen, D.; Huang, C.; Morgenroth, E.; Boppart,
- 501 S. A.; Ashbolt, N. J.; Liu, W.-T.; Nguyen, T. H., Role of Biofilm Roughness and Hydrodynamic
- 502 Conditions in Legionella pneumophila Adhesion to and Detachment from Simulated Drinking
- Water Biofilms. Environmental science & technology 2015, 49 (7), 4274-4282.
- 504 18. Fortunato, L.; Qamar, A.; Wang, Y.; Jeong, S.; Leiknes, T., In-situ assessment of biofilm
- formation in submerged membrane system using optical coherence tomography and computational
- fluid dynamics. *Journal of Membrane Science* **2017**, *521*, 84-94.

- 507 19. Xi, C.; Marks, D.; Schlachter, S.; Luo, W.; Boppart, S. A., High-resolution three-
- dimensional imaging of biofilm development using optical coherence tomography. J Biomed Opt
- **2006,** *11* (3), 34001.
- 510 20. Hou, J.; Wang, C.; Rozenbaum, R. T.; Gusnaniar, N.; de Jong, E. D.; Woudstra, W.;
- Geertsema-Doornbusch, G. I.; Atema-Smit, J.; Sjollema, J.; Ren, Y.; Busscher, H. J.; van der
- 512 Mei, H. C., Bacterial Density and Biofilm Structure Determined by Optical Coherence
- 513 Tomography. *Scientific Reports* **2019**, *9* (1), 9794.
- 514 21. Walters, M. C., 3rd; Roe, F.; Bugnicourt, A.; Franklin, M. J.; Stewart, P. S., Contributions
- of antibiotic penetration, oxygen limitation, and low metabolic activity to tolerance of
- 516 Pseudomonas aeruginosa biofilms to ciprofloxacin and tobramycin. Antimicrob Agents Chemother
- **2003,** *47* (1), 317-323.
- Nerenberg, R., The membrane-biofilm reactor (MBfR) as a counter-diffusional biofilm
- 519 process. Curr Opin Biotechnol **2016**, *38*, 131-6.
- 520 23. Reichhardt, C.; Parsek, M. R., Confocal Laser Scanning Microscopy for Analysis of
- 521 Pseudomonas aeruginosa Biofilm Architecture and Matrix Localization. Frontiers in
- 522 *Microbiology* **2019**, *10* (677).
- 523 24. Shen, Y.; Huang, C.; Monroy, G. L.; Janjaroen, D.; Derlon, N.; Lin, J.; Espinosa-Marzal,
- R.; Morgenroth, E.; Boppart, S. A.; Ashbolt, N. J.; Liu, W.-T.; Nguyen, T. H., Response of
- 525 Simulated Drinking Water Biofilm Mechanical and Structural Properties to Long-Term
- 526 Disinfectant Exposure. Environmental Science & Technology 2016, 50 (4), 1779-1787.
- 527 25. Shen, Y.; Huang, P. C.; Huang, C.; Sun, P.; Monroy, G. L.; Wu, W.; Lin, J.; Espinosa-
- 528 Marzal, R. M.; Boppart, S. A.; Liu, W.-T.; Nguyen, T. H., Effect of divalent ions and a
- 529 polyphosphate on composition, structure, and stiffness of simulated drinking water biofilms. npj
- 530 *Biofilms and Microbiomes* **2018,** *4* (1), 15.
- 531 26. Shen, Y.; Huang, C.; Lin, J.; Wu, W.; Ashbolt, N. J.; Liu, W.-T.; Nguyen, T. H., Effect
- of disinfectant exposure on Legionella pneumophila associated with simulated drinking water
- biofilms: release, inactivation, and infectivity. *Environmental Science & Technology* **2017**.
- 534 27. Tierra, G.; Pavissich, J. P.; Nerenberg, R.; Xu, Z.; Alber, M. S., Multicomponent model
- of deformation and detachment of a biofilm under fluid flow. J R Soc Interface 2015, 12 (106).
- 536 28. Abe, Y.; Polyakov, P.; Skali-Lami, S.; Francius, G., Elasticity and physico-chemical
- properties during drinking water biofilm formation. *Biofouling* **2011,** *27* (7), 739-750.
- 538 29. Peterson, B. W.; He, Y.; Ren, Y.; Zerdoum, A.; Libera, M. R.; Sharma, P. K.; van
- Winkelhoff, A.-J.; Neut, D.; Stoodley, P.; van der Mei, H. C.; Busscher, H. J., Viscoelasticity of
- 540 biofilms and their recalcitrance to mechanical and chemical challenges. FEMS Microbiology
- 541 Reviews **2015**, *39* (2), 234-245.
- 542 30. Zeng, G.; Vad, B. S.; Dueholm, M. S.; Christiansen, G.; Nilsson, M.; Tolker-Nielsen,
- 543 T.; Nielsen, P. H.; Meyer, R. L.; Otzen, D. E., Functional bacterial amyloid increases
- Pseudomonas biofilm hydrophobicity and stiffness. Frontiers in Microbiology **2015**, 6 (1099).
- 545 31. Shaw, T.; Winston, M.; Rupp, C. J.; Klapper, I.; Stoodley, P., Commonality of Elastic
- Relaxation Times in Biofilms. *Physical Review Letters* **2004**, *93* (9), 098102.
- 547 32. Fish, K.; Osborn, A. M.; Boxall, J. B., Biofilm structures (EPS and bacterial communities)
- in drinking water distribution systems are conditioned by hydraulics and influence discolouration.
- 549 *Science of The Total Environment* **2017,** *593-594*, 571-580.
- 550 33. Sanz-Herrera, J. A.; García-Aznar, J. M.; Doblaré, M., On scaffold designing for bone
- regeneration: A computational multiscale approach. *Acta Biomaterialia* **2009,** *5* (1), 219-229.

- 552 34. Lin, C. Y.; Kikuchi, N.; Hollister, S. J., A novel method for biomaterial scaffold internal
- architecture design to match bone elastic properties with desired porosity. *Journal of Biomechanics*
- **2004,** *37* (5), 623-636.
- 555 35. Torres-Sanchez, C.; Al Mushref, F. R. A.; Norrito, M.; Yendall, K.; Liu, Y.; Conway, P.
- P., The effect of pore size and porosity on mechanical properties and biological response of porous
- 557 titanium scaffolds. *Materials Science and Engineering: C* **2017,** 77, 219-228.
- 558 36. Hozalski, R. M.; Esbri-Amador, E.; Chen, C. F., Comparison of stannous chloride and
- phosphate for lead corrosion control. *Journal AWWA* **2005,** 97 (3), 89-103.
- 560 37. Mahmoud, B.; Zhe, X.; Leah, G.; Yingjie, D.; Hongbing, L.; Philippe, Z.; Majid, M.-J.,
- Nanoindentation of Pseudomonas aeruginosa bacterial biofilm using atomic force microscopy.
- 562 *Materials Research Express* **2014,** *I* (4), 045411.
- 563 38. Andrews, J. W.; Bowen, J.; Cheneler, D., Optimised determination of viscoelastic
- properties using compliant measurement systems. *Soft Matter* **2013**, *9* (23), 5581-5593.
- 565 39. Lau, P. C. Y.; Dutcher, J. R.; Beveridge, T. J.; Lam, J. S., Absolute Quantitation of
- Bacterial Biofilm Adhesion and Viscoelasticity by Microbead Force Spectroscopy. *Biophysical*
- 567 Journal **2009**, 96 (7), 2935-2948.
- 568 40. Thomas, G.; Burnham, N. A.; Camesano, T. A.; Wen, Q., Measuring the Mechanical
- Properties of Living Cells Using Atomic Force Microscopy. Journal of Visualized Experiments:
- 570 *JoVE* **2013**, (76), 50497.
- 571 41. Lee, J.-J.; Rao, S.; Kaushik, G.; Azeloglu, E. U.; Costa, K. D., Dehomogenized Elastic
- 572 Properties of Heterogeneous Layered Materials in AFM Indentation Experiments. Biophysical
- 573 Journal 2018, 114 (11), 2717-2731.
- Huang, P.; Chaney, E. J.; Shelton, R. L.; Boppart, S. A., Magnetomotive Displacement of
- 575 the Tympanic Membrane Using Magnetic Nanoparticles: Toward Enhancement of Sound
- Perception. *IEEE Transactions on Biomedical Engineering* **2018**, *65* (12), 2837-2846.
- 577 43. Schindelin, J.; Arganda-Carreras, I.; Frise, E.; Kaynig, V.; Longair, M.; Pietzsch, T.;
- Preibisch, S.; Rueden, C.; Saalfeld, S.; Schmid, B.; Tinevez, J.-Y.; White, D. J.; Hartenstein,
- V.; Eliceiri, K.; Tomancak, P.; Cardona, A., Fiji: an open-source platform for biological-image
- 580 analysis. *Nature Methods* **2012**, *9* (7), 676-682.
- Derlon, N.; Peter-Varbanets, M.; Scheidegger, A.; Pronk, W.; Morgenroth, E., Predation
- influences the structure of biofilm developed on ultrafiltration membranes. Water Res 2012, 46
- 583 (10), 3323-33.
- 584 45. Gerke, K. M.; Vasilyev, R. V.; Khirevich, S.; Collins, D.; Karsanina, M. V.; Sizonenko,
- 585 T. O.; Korost, D. V.; Lamontagne, S.; Mallants, D., Finite-difference method Stokes solver
- 586 (FDMSS) for 3D pore geometries: Software development, validation and case studies. *Computers*
- 587 & Geosciences **2018**, 114, 41-58.
- 588 46. Carrel, M.; Morales, V. L.; Beltran, M. A.; Derlon, N.; Kaufmann, R.; Morgenroth, E.;
- Holzner, M., Biofilms in 3D porous media: Delineating the influence of the pore network geometry,
- flow and mass transfer on biofilm development. Water Research 2018, 134, 280-291.
- 591 47. Sekhon, J. S., Multivariate and Propensity Score Matching Software with Automated
- Balance Optimization: The Matching package for R. 2011 2011, 42 (7), 52.
- 593 48. Lieleg, O.; Caldara, M.; Baumgärtel, R.; Ribbeck, K., Mechanical robustness of
- Pseudomonas aeruginosa biofilms. *Soft matter* **2011,** *7* (7), 3307-3314.
- 895 49. Rushing, J. C.; McNeill, L. S.; Edwards, M., Some effects of aqueous silica on the
- 596 corrosion of iron. *Water Research* **2003**, *37* (5), 1080-1090.

- 597 50. Gao, H.; Li, Q.; Chen, F. N.; Dai, Y.; Luo, F.; Li, L. Q., Study of the corrosion inhibition
- effect of sodium silicate on AZ91D magnesium alloy. *Corrosion Science* **2011**, *53* (4), 1401-1407.
- 599 51. Ammar, Y.; Swailes, D.; Bridgens, B.; Chen, J., Influence of surface roughness on the initial formation of biofilm. *Surface and Coatings Technology* **2015**, *284*, 410-416.
- 601 52. Kundukad, B.; Seviour, T.; Liang, Y.; Rice, S. A.; Kjelleberg, S.; Doyle, P. S.,
- Mechanical properties of the superficial biofilm layer determine the architecture of biofilms. Soft
- 603 *Matter* **2016,** *12* (26), 5718-5726.
- 53. Savchenko, N.; Sevostyanova, I.; Sablina, T.; Gömze, L.; Kulkov, S., The influence of
- 605 porosity on the elasticity and strength of alumina and zirconia ceramics. AIP Conference
- 606 Proceedings **2014**, 1623 (1), 547-550.
- Vreeburg, I. J. H. G.; Boxall, D. J. B., Discolouration in potable water distribution systems:
- 608 A review. Water Research 2007, 41 (3), 519-529.
- 609 55. Falkinham, J. O.; Pruden, A.; Edwards, M., Opportunistic Premise Plumbing Pathogens:
- Increasingly Important Pathogens in Drinking Water. Pathogens (Basel, Switzerland) 2015, 4 (2),
- 611 373-386.
- 612 56. Feazel, L. M.; Baumgartner, L. K.; Peterson, K. L.; Frank, D. N.; Harris, J. K.; Pace, N.
- R., Opportunistic pathogens enriched in showerhead biofilms. Proceedings of the National
- 614 Academy of Sciences **2009**, 106 (38), 16393-16399.
- 615 57. Lehtola, M. J.; Torvinen, E.; Kusnetsov, J.; Pitkänen, T.; Maunula, L.; von Bonsdorff,
- 616 C.-H.; Martikainen, P. J.; Wilks, S. A.; Keevil, C. W.; Miettinen, I. T., Survival of
- Mycobacterium avium, Legionella pneumophila, Escherichia coli, and Caliciviruses in Drinking
- Water-Associated Biofilms Grown under High-Shear Turbulent Flow. Applied and Environmental
- 619 *Microbiology* **2007,** *73* (9), 2854-2859.
- 620 58. Wang, H.; Edwards, M.; Falkinham, J. O.; Pruden, A., Molecular Survey of the
- Occurrence of Legionella spp., Mycobacterium spp., Pseudomonas aeruginosa, and Amoeba Hosts
- 622 in Two Chloraminated Drinking Water Distribution Systems. Applied and Environmental
- 623 *Microbiology* **2012**, *78* (17), 6285-6294.